NASA Technical Memorandum 100056

A Method of Atmospheric Density Measurements During Space Shuttle Entry Using Ultraviolet-Laser Rayleigh Scattering

Robert L. McKenzie

(NASA-TM-100056) A METHOD OF ATMOSPHERIC DENSITY MEASUREMENTS DURING SPACE SHUTTLE ENTRY USING ULTRAVIOLET-LASER RAYLEIGH SCATTERING (NASA) 37 p CSCL 14B

N88-22337

Unclas

G3/35 0140766

March 1988

National Aeronautics and Space Administration

NASA Technical Memorandum 100056

A Method of Atmospheric Density Measurements During Space Shuttle Entry Using Ultraviolet-Laser Rayleigh Scattering

Robert L. McKenzie, Ames Research Center, Moffett Field, California

March 1988

National Aeronautics and
Space Administration

Ames Research Center
Moffett Field, California 94035

A METHOD OF ATMOSPHERIC DENSITY MEASUREMENTS DURING SPACE SHUTTLE ENTRY USING ULTRAVIOLET-LASER RAYLEIGH SCATTERING

Robert L. McKenzie*
NASA Ames Research Center, Moffett Field, California

Abstract

An analytical study and its experimental verification are described which show the performance capabilities and the hardware requirements of a method for measuring atmospheric density along the Space Shuttle flightpath during entry. Using onboard instrumentation, the technique relies on Rayleigh scattering of light from a pulsed ArF excimer laser operating at a wavelength of 193 nm. The method is shown to be capable of providing density measurements with an uncertainty of less than 1% and with a spatial resolution along the flightpath of 1 km, over an altitude range from 50 to 90 km. Experimental verification of the signal linearity and the expected signal-to-noise ratios is demonstrated in a simulation facility at conditions that duplicate the signal levels of the flight environment.

Introduction

Over the altitude range from 50 to 100 km, where the Space Shuttle is at an angle of attack for maximum aerodynamic braking, meteorological fluctuations in the atmosphere density are also their greatest. As Fig. 1 shows, unpredictable departures from the 1976 Standard Atmosphere[1] may reach extremes as large as 80% with a 1% probability. The scale of the disturbances have been evaluated from radiosonde data[2-4] which show the presence of discrete layers of turbulence with a minimum thickness of tens of meters and with vertical wavelengths of about 1 km. Similar results have been derived from accelerometer data taken during the first 12 Space Shuttle flights.[5] Those data indicate that the flights encountered extreme density variations from -55% to +10% at altitudes from 80 to 100 km and abrupt density changes of 15-20% over vertical distances of less than 1 km.

*Research Scientist, Associate Fellow AIAA.

The uncertainty with which these ambient density variations are measured along the entry flightpath can directly affect the evaluation of the Shuttle's aerodynamic coefficients from dynamic flight data. The density uncertainties can obscure the contributions of such factors as real gas effects and full-scale viscous effects which influence the aerodynamic coefficients in flight but are not accurately represented in wind tunnel measurements. Moreover, in the low-density transition regime between free-molecule and continuum flow, even the ratios of forces such as lift-to-drag, are density-dependent. For Shuttle trajectories, this transition regime occurs in the altitude range between 80 and 140 km.[6] Finally, accurate measurements along the Space Shuttle flightpath will also contribute to upper atmosphere meteorological data at altitudes that are much higher than those which are accessible to balloon-borne instruments. Density variations in the mesosphere (50-90 km) have gained recent interest for the analysis of uncertainties in the exit trajectories of orbital aero-braking vehicles.[7]

Presently, determinations of upper atmosphere densities along the flight-path of the Shuttle are obtained by a variety of methods including measurements by radiosondes and rocket-launched meteorological spheres,[8] by accelerometer data taken from instruments on-board the Shuttle and used in combination with radiosondes and other flight data,[6,9] and by instrumentation that samples air data from the surface of the vehicle.[10-12] The methods are summarized in Table I along with estimates of their uncertainty in the determination of density over the altitude range of their applicability.

None of the methods which are currently available are able to measure density along the flight path both directly and at the time of flight. Only the radiosondes and rocketsondes provide a direct measurement of density, but the results must be extrapolated to the time and location of the entry vehicle flightpath.[8] Best-estimated-trajectories (BET) are obtained by combining on-board Inertial Measurement Unit (IMU) accelerometer data with radiosonde data,[9] but the use of IMU/BET to imply values of atmospheric density also requires a detailed and accurate knowledge of the vehicle aerodynamic force coefficients at the particular flight speed, angle of attack, and control surface configuration for each point along the trajectory. For example, the 3-5% density uncertainty which is shown in Table 1 for the IMU/BET

determinations reflects the magnitude of an apparent variation from the standard normal-force coefficients given by the Orbiter Aerodynamic Data Base.[5]

To date, the most accurate determination of atmospheric density which has been obtained from flight data in the continuum-flow regime has come from the Shuttle Entry Air Data System (SEADS).[10,11] It measures pressures on the nose of the airframe using an array of surface orifices. An analysis of the data relies on an independent knowledge of the aerodynamics of the nose flow and leads to determinations of the dynamic pressure and the angle of attack with uncertainties of 3% and 0.3°, respectively.[13] Although dynamic pressure is the primary variable of interest for the determination of aerodynamic force coefficients, atmospheric density has also been extracted from the data with an uncertainty of 3 to 4%.

Table 1 also includes on-board instrumentation giving atmospheric densities at higher altitudes where low-density-flow effects are prevalent.[6,12] However, much greater uncertainties accompany the results and are again partly a consequence of the uncertainty in aerodynamic force coefficients.

In this paper, the performance capabilities and the hardware requirements are described for a technique in which atmospheric density along the Shuttle flight path is measured using on-board laser-based instrumentation. The principal objectives are to provide direct and more accurate measurements of atmospheric density over a maximum range of altitudes including those where the greatest meteorological variations in the atmosphere occur. In addition, measurements are desirable having a spatial resolution which is adequate to allow the detection of the small-scale meteorological structure that may influence the flight dynamics of an entry vehicle and the analysis of upper atmosphere meteorology.

The introduction of laser-based instrumentation on-board the Shuttle will also lay the foundation for more advanced measurements within the shock layer, in support of aerothermodynamic studies and computer model verification for advanced entry vehicle design. The feasibility of such measurements based on current technology is discussed in Ref. 14 for several extensions to this concept. They provide density profiles within the shock layer during entry, using the same laser system which is described here for atmospheric density measurements.

This technique relies on the Rayleigh scattering of light from a pulsed ultraviolet laser. The laser beam emerges from the window in the mid-deck crew hatch and propagates in a direction which is nearly normal to the longitudinal body-axis of the vehicle. Light scattered backward by the ambient air is collected during each pulse by optics attached to the inside of the window. The collection optics are arranged so that only light scattered from the length of the beam that is beyond the shock layer is detected. The intensity of the scattered light is time-integrated over a selected period following each laser pulse to obtain a signal that is a measure of the total energy of light scattered during that period. The signal, which is normalized by the laser pulse energy, is linearly proportional to the atmospheric density in the observed length of the beam and has no significant dependence on any other properties of the atmosphere or on the flight conditions.

Requirements and Limiting Factors

To establish the altitude and spatial-resolution requirements for these measurements, the radiosonde[2-4] data and the Shuttle flight data[5] show that altitudes at least up to 80 km must be included if the largest density variations are to be detected. To encompass the low-density flight regime, altitudes to 100 km would be preferred. The data also suggest that a spatial resolution of 1 km or less is required to adequately define the small-scale structure that has been observed. Thus, for this application, the chosen measurement goals are to achieve a measurement uncertainty of less than 1% at altitudes greater than 80 km and with a spatial resolution along the flight path better than 1 km.

The uncertainty of an optical measurement is usually characterized by its overall signal-to-noise ratio (SNR). If $\bar{N}_{atm}$ denotes the local atmospheric number density averaged over the temporal or spatial interval of its measurement and ΔN_{atm} is the rms standard deviation (uncertainty) in the measurement, then the relative uncertainty of the measurement is $\Delta N_{atm}/\bar{N}_{atm}$ and the overall SNR is defined by

$$SNR = \bar{N}_{atm}/\Delta N_{atm} \qquad (1)$$

Thus, to obtain an uncertainty of less than 1%, the SNR must be greater than 100.

The uncertainty in the measurement arises, in part, from photon-statistical noise that is an unavoidable feature of any photo-detection process. It is equal to the square root of the total number of photoelectrons produced in the detector from all sources during a measurement time-interval. Possible contributing light sources include the Rayleigh-scattered light plus direct Sun light and Sun light scattered by the atmosphere, the cloud tops, and the Earth's surface albedo. In addition, aerosols and dust in the atmosphere scatter light in a manner that is indistinguishable from Rayleigh scattering. This particle scattering must also be included both as a component to the photon-statistical noise and as an uncertainty in the determination of atmospheric density which is derived from the total signal.

Since the photon-statistical noise is related to the total number of photoelectrons that are accumulated during a measurement interval, the signal is most conveniently described in the same way. Hence, the total signal is defined as equal to the total number of photoelectrons that are produced by the Rayleigh scattered light during a measurement interval. To separate the Rayleigh contribution from the total signal, the flight instrumentation must include a separate measurement of the continuous background light, made in a time-interval between laser pulses when no Rayleigh scattering is present. This measurement can be made using simple electronic gating of the signal from the same photodetector that is used to observe the Rayleigh signal.

The noise increases only as the square root of the total signal so that the SNR increases as the Rayleigh signal increases. The Rayleigh signal can be maximized both by increasing the Rayleigh scattered light produced by a single laser pulse and by summing the single-pulse signals over a number of pulses. Since the number of accumulated pulses will be limited to the number that occur within the time that is necessary to travel a specified distance along the flightpath, the specified spatial resolution along the flightpath will limit the SNR and encourage the use of a high-average-power laser.

Instrumentation Design

Rayleigh Scattering

The use of Rayleigh scattering is attractive because it is the simplest of all radiative interactions with gases. The scattered light is at nearly the same wavelength and bandwidth as the source, its intensity is proportional to the number density of the medium, but it is insensitive to the temperature of the medium. The cross-section for Rayleigh scattering is strongly dependent on wavelength but, in the case of backward scattering from gases, the intensity of scattered light is independent of the polarization of the incident light. Furthermore, in air at ambient temperatures, the photon yield for Rayleigh scattering is greater than that from any other radiative interaction including laser-induced fluorescence. Hence, the optical signal is maximum while the requirements on the laser energy and its spectral qualities are minimum.

The magnitude of the Rayleigh signal can be related to the physical properties of the laser and to the parameters of the collection optics by first describing the power of light scattered in the backward direction from a volume, V, into an element of solid angle, $d\Omega$. The result is[15]

$$\frac{\partial P_s}{\partial \Omega} = \frac{P_L}{A_L} \bar{N}_{atm} V \left(\frac{2}{2 + \rho_n} \right) \frac{\partial \sigma}{\partial \Omega} \tag{2}$$

where P_L/A_L is the power-per-unit-area of the incident laser radiation and $\partial\sigma/\partial\Omega$ is the differential Rayleigh cross-section. For most gases, the depolarization factor, ρ_n, is typically very small compared to unity.[16] ($\rho_n = 0.02$ for N_2 and 0.06 for O_2.) Hence, for this application, the term in brackets is assumed equal to unity.

The differential Rayleigh cross section varies with the scattering direction according to

$$\frac{\partial \sigma}{\partial \Omega} = \sigma_o \frac{1}{2} (1 + \cos^2 \psi) \tag{3}$$

where ψ is the azimuthal scattering angle. Thus, for backward scattering, $\psi = 180°$ and $\partial\sigma/\partial\Omega = \sigma_o$. Frequently, the coefficient, σ_o, is referred to as the Rayleigh cross section and that description is adopted here. The Rayleigh cross-section varies with wavelength, λ, according to

$$\sigma_o = \frac{4\pi^2}{\lambda^4}\left(\frac{n_{stp} - 1}{N_{stp}}\right)^2 \qquad (4)$$

where n_{stp} is the refractive index of air at standard temperature and pressure and N_{stp} is the corresponding number density. Corrections to Eq.(4) to account for variations of the term, $(n_{stp} - 1)/N_{stp}$, with temperature can be shown to be negligible for this application.[17]

The effects of ultraviolet resonances on the Rayleigh cross section is also a consideration, particularly for O_2 which has absorption transitions that fall within the bandwidth of the ArF laser centered at 193 nm. Dispersion data for air, which define the variation of refractive index with wavelength and can be related to the Rayleigh cross section, show no significant resonant effects at ultraviolet wavelengths down to 185 nm.[18] That conclusion is supported further by calculations[19] based on recent values of the oscillator strengths[20-21] for O_2 which indicate that the resonance enhancement should be much less than 1%. Consequently, the cross-section measurements reported in Ref. 16 for O_2 and N_2 at wavelengths down to 364 nm have been used to compute a cross-section parameter for air (79% N_2, 21% O_2) of $\lambda^4\sigma_o = 4.81 \times 10^{-17}$ nm^4 cm^2.

For pulsed applications, Eq.(2) may be integrated over the solid angle, $\Omega(x)$, of light collected from each position, x, along the laser beam and over the duration of the signal pulse. It may also be divided by the energy per photon, hc/λ, to cast the expression in terms of the total number of scattered photons per pulse. The single-pulse Rayleigh signal (S_{Ray} in Eq. (5)) is then obtained by multiplying by the the quantum efficiency of the photodetector and by the efficiency of the collection optics. Both efficiencies are combined into the parameter, η. The result is

$$S_{Ray} = \frac{\lambda}{hc}\,\sigma_o \bar{N}_{atm} E_L\,\eta \int \Omega(x)dx \qquad \text{(photoelectrons per pulse)} \qquad (5)$$

where E_L is the single-pulse energy of the laser.

Optical Configuration

The Rayleigh signal is maximized by observing the greatest length of laser beam possible. A co-axial Cassegrain arrangement of the type shown in

Fig. 2 accomplishes that objective by collecting back-scattered light from the entire beam which propagates beyond the range-limiting ray. The co-axial arrangement also eliminates the need for any critical alignment with the laser beam. With perfect alignment, such an arrangement also rejects scattered light from within the shock layer. Finally, the use of the folded optics provided by a Cassegrain arrangement minimizes the size of the optical apparatus that must be mounted inside the cabin window.

To define the relevant parameters of the collection optics, the diameter of the primary mirror is denoted as d_p, the diameter of the secondary mirror is d_s, and x_o is the point on the laser beam that is intersected by the range-limiting ray. The clear aperture area of the collection optics is then $A_c = (d_p^2 - d_s^2)\pi/4$ and the solid angle for light collection from x to $x + dx$ can be accurately approximated by $\Omega(x) \approx A_c/x^2$ for all values of x where $4x^2/d_p^2 >> 1$. Equation (5) may then be integrated from $x = x_o$ to ∞ with the result

$$S_{Ray} = \frac{\lambda}{hc}\,\sigma_o \bar{N}_{atm} E_L \eta\,\frac{A_c}{x_o} \qquad (6)$$

Values of the minimum range, x_o, are dictated by the Space Shuttle flow field. While the vehicle is in hypersonic flight (Mach no. > 5, altitude > 40 km) the maximum shock layer thickness in the direction of the laser beam is estimated to be less than 200 cm.[22-24] Hence, this design is based on $x_o = 200$ cm. The size of the hatch window limits the aperture diameter of the collection optics to $d_p = 23$ cm.

With these constraints, a final configuration was chosen in which the primary mirror diameter is $d_p = 22.86$ cm with a focal length of 23 cm, the secondary mirror diameter is $d_s = 11.44$ cm with a focal length of 30 cm, and their separation is 13.7 cm. For the experiment, prototype spherical mirrors were fabricated with UV-enhanced aluminum coatings having a reflectivity per surface of 88% at a wavelength of 193 nm.

Figure 2 also shows the crew-hatch window to have three panes. The window material is uncoated UV-grade fused silica. The total transmission of the window set, including absorption and reflection losses from the six surfaces is 61% at 193 nm. Also note that the laser beam is transmitted through separate central windows in each pane which are optically isolated from the

outer segments by a beam tube. This configuration is required to eliminate the large signals caused by Rayleigh-scattered light in the window material which would travel radially outward within the window and scatter into the collection optics. Initial experiments showed this feature to be essential.

From the foregoing description, the collection optics have á total collection efficiency of 35%, not including the quantum efficiency of the photodetector. The laboratory version has an overall length of 40 cm, including the detector housing and the mirror mounts.

Laser Selection

The relevant parameter defining the laser performance for this application is its average power. Pulsed lasers are generally superior to continuous-wave lasers for obtaining high average power, particularly in the ultraviolet spectral regions. Hence, they are the primary candidates for this application.

The major factors contributing to the selection of a laser are illustrated in Fig. 3. For example, by combining Eqs. (4) and (5), the wavelength dependence of the Rayleigh signal can be shown to be proportional to $1/\lambda^3$ when the signal is measured in terms of photoelectrons per pulse. This feature of Rayleigh scattering is shown by Fig. 3 to encourage the use of the shortest wavelength possible. Further encouragement is given by the rapid decrease in solar radiation with wavelength in the ultraviolet spectral region, also shown in Fig. 3. On the other hand, a practical lower limit in wavelength is dictated by the radiative absorption of the window material, as shown in Fig. 3 by the transmission curve for UV-grade fused silica.

The wavelengths of two ultraviolet lasers are also indicated in Fig. 3. They represent the choices with the shortest acceptable wavelengths that can be obtained from current laser technology with comparatively high average power.

The ArF excimer laser, operating at 193 nm, is most ideal because its wavelength falls closest to the transmission limit. Commercial units are available that can provide repetition rates exceeding 200 Hz, pulse energies exceeding 200 mJ, thereby giving average powers reaching 60 W.[25] On the other hand, the laser and its power supply is typically large (150 cm long) and

heavy (250 kg). Moreover, it requires high electrical power (1-3 kW) and it relies on toxic gases (Fluorine).

The second candidate, a frequency-quadrupled Nd:YAG solid-state laser operating at 266 nm, is commercially available with sizes and weights that are smaller than most excimer lasers and it requires no gases. However, the electrical power requirements for the presently available flash-lamp-excited versions can be equally large. The newest technology now uses diode-laser-excited devices which are not yet available commercially with high average powers but may eventually provide significant reductions in electrical power requirements. On the other hand, commercial Nd:YAG lasers operating at 266 nm are typically limited to pulse energies up to 20 mJ and to repetition rates up to 30 Hz, thereby giving maximum average powers up to only 0.6 W. Nevertheless, these limits are within a range that is worthy of evaluation and they do not represent the maximum capabilities that might be obtained from such a system. Consideration of the Nd:YAG laser for this application is compelling because its installation in the Space Shuttle would be less imposing.

Lasers operating at longer wavelengths, with greater average powers than either of the two choices above were found not to be competitive because of the smaller SNR resulting from a smaller Rayleigh cross-section in combination with a larger solar background and particle scattering signal.

Performance

With the collection optics and the laser parameters already defined, the remaining factors that influence the overall SNR include the detector characteristics, the signal integration period, the intensity of the solar background, and the competition with the Rayleigh signal by particle scattering. In the paragraphs to follow, each of these factors is evaluated and then combined into an overall SNR expression.

Detector Characteristics

The parameters used here that characterize the photodetector are modeled after a commercial eight-stage photomultiplier with a CsTe solar-blind photocathode and a UV-transmitting fused silica envelope. The spectral response of the photosurface is nearly uniform over the wavelength range between 193 and

266 nm and corresponds to a quantum efficiency of 15%. The relevant electrical features of the photomultiplier tube (PMT) are summarized in Table 2.

An optical interference filter with its bandpass centered on the laser wavelength is also incorporated to reduce the photon-statistical noise that is contributed by the solar background. The filter parameters are also included in Table 2.

Signal Integration

The time-dependent Rayleigh signal waveform depends on the position, x, of the outward propagating laser pulse and decreases as $1/x^2$. The time-integrated signal is maximized by integrating the waveform over a period that extends to infinity, as was done to obtain Eq. (5). However, continuous solar background radiation also reaches the detector during the same integration period and contributes to the accumulated photon-statistical noise. Consequently, the integration period should be terminated when the integral has approached its full value. In addition, light that is multiply-scattered by particles and optical surfaces at close range is never completely rejected by the Cassegrain optical arrangement. Some spurious light can reach the detector in the early time period before the tail of the laser pulse has cleared the minimum range, x_o. To eliminate the risk of such spurious signals, the integration period is not started until after the laser pulse has cleared x_o, at the expense of an additional loss of integrated signal.

Detailed calculations have been performed that simulate the time-dependent waveform of the Rayleigh scattering signal. The results show that if the integration period is started after the time at which the entire 16-ns laser pulse is beyond x_o, and is continued to the time when 90% of the remaining integral has been received, the integration period is Δt = 80 ns and the acquired integral is 54% of the value obtained by integrating over all time. This feature is included in the performance calculations to follow, as a conservative measure.

Solar background

The contributions to solar background that are considered in this application correspond to flight maneuvers in which the Shuttle is either rolled to a position where the Sun is directly in view of the collection optics, one in

which the field of view is downward and filled entirely by the Earth's surface, or one in which the horizon is in view and the Sun is behind the observer. In the latter two cases, the background will include the light scattered by the atmosphere. The background signal in all cases is proportional to the solar flux that is transmitted by the detector filter. For these calculations, the solar flux was taken from the Solar Spectral Irradiance Standard Curve[26] and convolved with a filter transmission curve centered at each laser wavelength.

For a filter bandpass centered at 193 nm, in which the transmitted solar flux is smallest, direct observation of the Sun was found to produce a continuous signal that exceeds the maximum average-anode-current of the PMT by several orders of magnitude. Hence, direct solar observation must always be avoided. That can be accomplished easily by including a small shutter in front of the PMT that closes when the image of the Sun approaches the edge of the detector aperture.

To evaluate the background signals for a downward or horizontal-looking position, radiance values for solar scattering in a backward direction by the atmosphere are taken from Monte Carlo calculations for wavelengths down to 270 nm.[27] The calculations include the effects of ozone absorption, multiple-scattering including Rayleigh and aerosol contributions, and surface albedo. The results show that for wavelengths below 300 nm, ozone absorption is the largest contributor to the loss of incident solar irradiance and its subsequent scattering. As a consequence, solar light at those wavelengths does not reach the lower atmosphere, the cloud tops, or the Earth's surface. The scattering intensity in all directions is then independent of cloud or surface albedo. The calculations also show that the scattered radiance is dominated by Rayleigh scattering and that it can be 2 to 10 times larger from the horizon then from the nadir, depending on the position of the Sun. At a wavelength of 270 nm, the maximum fraction of solar flux that appears as scattered radiance from the horizon is estimated to be $R_{solar} = 2 \times 10^{-4}$. Since ozone absorption and the Rayleigh scattering cross-section both increase when going from 270 nm to 193 nm, the two effects are compensating. Hence, the same radiance value was assumed for 193 nm.

The solar flux is also assumed to be back-scattered uniformly into 2π-steradians. Moreover, for a solar background in which no contribution from

surface scattering occurs, altitude is not a relevant parameter. The scattered light appears to come from an extended field that fills the field of view. Thus, if Ω_c is the solid angle that defines the field of view for light entering the aperture area, A_c, then the effective aperture area is $A_c/(1 - \Omega_c/4\pi)$ and the solar background signal is given by

$$S_{solar} = I_{filter} R_{solar} \Delta t \, \eta \, \frac{A_c}{1 - \Omega_c/4\pi} \tag{7}$$

where I_{filter} is the solar flux (photons/cm^2 sec) that is transmitted by the filter and Δt is the integration period used for the Rayleigh signal. For the optical system used here, A_c=308 cm, and $\Omega_c/4\pi = (d_p/4x_o)^2 = 8.3 \times 10^{-4}$.

Calculations using Eq. (7) show that while the solar background at λ = 193 nm is not large, it becomes a significant contributor to the measurement uncertainty at λ = 266 nm.

Particle Scattering

At lower altitudes, the competition of particle scattering with the Rayleigh scattering becomes the major factor that contributes to the uncertainty. It thereby limits the lowest altitude at which this concept can be applied. Unfortunately, an estimation of particle scattering by atmospheric aerosols is a complex problem which is not predicted as accurately as it is for gaseous Rayleigh scattering. Furthermore, most of the detailed studies of atmospheric particle scattering have been confined to altitudes below 30 km where it is most significant. Therefore, to estimate the effects of particle scattering at altitudes up to 100 km, a very approximate approach has been taken for determining the scattering cross-section but it allows realistic models for the particle size distribution and for the particle density variations with altitude to be included easily. The accuracy of the predictions is then evaluated by comparing them to recent LIDAR measurements of aerosol scattering at altitudes up to 30 km.

To that end, the signal owing to particle scattering may also be described by Eq. (6) except that the Rayleigh cross-section is replaced by an average particle cross-section that depends on the distribution of particle sizes. The expressions that are used here for the cross-sections pertain to the total amount of light scattered into 4π-steradians. Since the intensity

of light scattered by particles in the backward direction is known to be 10^{-3} to 10^{-1} of the intensity in the forward direction,[28] the total cross-sections used here are a closer representation of the forward-scattered intensity and should lead to an over-prediction of the back scattering. On the other hand, these arguments pertain to single-particle scattering. The degree of over-prediction is expected to be offset by the equally undetermined and opposite effects of multiple scattering, which will re-direct some of the light that is scattered forward into the backward direction.

In view of the considerations above, the total scattering cross-section for transparent spherical particles with a radius, r, that is much smaller than λ (i.e., $2\pi r/\lambda << 1$), is given by[28]

$$\sigma_p' = \frac{8}{3}\left(\frac{n_p^2 - 1}{n_p^2 + 2}\right)^2\left(\frac{2\pi r}{\lambda}\right)^4 \pi r^2 \tag{8}$$

where n_p is the refractive index of the particle. Experimental data for aerosols at infrared wavelengths[29,30] show that $n_p = 1.5$ is a representative value.

For large particles where $2\pi r/\lambda >> 1$, the effective particle total cross section is independent of wavelength and is given approximately by[28]

$$\sigma_p'' = 2\pi r^2 \tag{9}$$

The average particle cross section for a distribution of particle sizes is then estimated for a given wavelength by

$$\sigma_p = \frac{1}{\bar{N}_p}\int_o^\infty N_r(r)\sigma(r,\lambda)dr \tag{10}$$

where $\bar{N}_p$ is the total particle density, N_r is the particle density in the range from r to $r + dr$, and the cross-section to be used in the integral is the smaller of the two values obtained from Eqs. (8) and (9).

A size-distribution given by the Haze-Model-C proposed by Deirmendjian[31] and slightly modified[29] has been used here to obtain $\sigma_p = 7.2 \times 10^{-10}$ cm^2 for both λ = 193 nm and 266 nm. The cross section is insensitive to wavelength in the ultraviolet spectrum because it is dominated by particle sizes where $2\pi r/\lambda >> 1$. The Haze-Model-C is assumed to be representative of

particle distributions at all altitudes from sea level to 100 km, with the exclusion of meteoric material having a radius less than 0.1 μm.[32] Since the average cross section used here is insensitive to scattering from such small particles, it is assumed to be applicable to all altitudes for the wavelengths considered.

The ratio of the signal contributed by particle scattering to that from Rayleigh scattering is then simply

$$\frac{S_{part}}{S_{Ray}} = \frac{\bar{N}_p \sigma_p}{\bar{N}_{atm} \sigma_o} \tag{11}$$

It is independent of all instrument parameters other than wavelength and it is a measure of the uncertainty in the atmospheric density measurement caused by particle scattering.

Values of the signal ratio given by Eq. (11) which are calculated using a recommended model[29] for the total particle densities at altitudes from sea level to 100 km and for $\lambda = 193$ nm have a peak ratio of 0.4 at 18 km. This result may be compared with LIDAR measurements[33] showing peaks ranging from 0.1 to 1 and occurring at altitudes from 15 to 20 km. However, the LIDAR measurements were made using a wavelength of 694 nm. If the experimental ratios are adjusted to correspond to 193 nm by simply accounting for the increase in Rayleigh cross section, they would be reduced by a factor of 46. However, the dependence of the aerosol back-scattering cross section on wavelength is uncertain so these predictions are left uncorrected as a conservative estimate. As a consequence, the predicted uncertainty which is imposed by particle scattering at $\lambda = 193$ nm exceeds 1% for all altitudes below 50 km, while for $\lambda = 266$ nm it will exceed 1% at all altitudes below 59 km because the Rayleigh signal is smaller.

The Overall Signal-to-Noise Ratio

To evaluate the SNR defined by Eq. (1), the total Rayleigh signal that is accumulated during a measurement interval in which n_{pulse} single-pulse signals are summed, may be computed from Eq. (5) with corrections to account for the truncated signal-integration period. The uncertainty associated with photon-statistical noise can then be determined from the fundamental relation for a

Poisson-statistical process that describes all photon-statistics.[34] The resulting rms noise amplitude is

$$N_{phot} = [n_{pulse}(S_{Ray} + S_{part} + S_{solar})]^{1/2} \quad (12)$$

The overall measurement uncertainty is the sum of contributions from the photon-statistical noise, which includes the particle scattering signal, and the uncertainty in the determination of density from the total signal, owing to particle scattering. Thus, the overall SNR may be estimated from

$$SNR = n_{pulse} S_{Ray}/(N_{phot} + n_{pulse} S_{part}) \quad (13)$$

The SNR values for three cases are plotted in Fig. 4 for altitudes up to 100 km. In one example, the performance of a frequency-quadrupled Nd:YAG laser and an ArF laser are compared when both lasers are operated at a single-pulse energy of 20 mJ and a repetition rate of 30 Hz. This comparison represents the case where both lasers are expected to require a similar amount of electrical power. It is limited by the maximum average power at which a commercial Nd:YAG laser can be operated at 266 nm, assuming both lasers have the same electrical efficiency. For a spatial resolution of 1 km and a flight speed of 6 km/sec, the 30-Hz repetition rate allows signals from five laser pulses to be summed.

As Fig. 4 shows, the performance of presently available Nd:YAG lasers is not adequate for this application and significant improvements would have to be achieved to make it adequate. The SNR at all altitudes is lower for λ = 266 nm primarily because of the smaller Rayleigh cross-section. Furthermore, the larger solar-background contribution to noise at 266 nm reduces the SNR by about a factor of two.

On the other hand, the ArF laser operating at the same accumulated energy, but with a shorter wavelength, is clearly capable of meeting the measurement goals. Moreover, the ArF laser can also be operated at a significantly higher average power with little loss in reliability and possibly without a major increase in size and weight. For example, operation at 50 mJ and 100 Hz can now be obtained from most commercial excimer lasers, which corresponds to an eight-fold increase in accumulated pulse energy along the

1-km flightpath. The resulting improvement in SNR and the extension of the altitude range is shown in Fig. 4.

From the results of these calculations, the most attractive choice for this application is an ArF laser that is capable of average powers approaching 5 W. Only the increased requirements for electrical power bring its selection into question. However, adequate electrical power is available aboard the Space Shuttle and little of it is in use during entry.

Shuttle Installation

Installation of the required laser system in the Space Shuttle will not be a minor project. Within the crew cabin, the collection optics and the beam tubes that enclose the path of the laser beam can all be mounted in place just prior to entry. The laser, its power supply, and its gas storage vessels can be self-contained within a volume of less than 1 cu. meter. Their combined weight is expected to be less than 300 kg. The required external utilities will include coolant flowing at 4 l/min and electrical power in the range between 1-3 kW.

The location of the laser may be selected from several options. In one configuration, the laser is located in the payload bay. The beam would then be brought into the cabin through a small sealed window assembly in the bulkhead and piped to the collection optics. This arrangement has the advantage that it minimizes the impact of the installation on the interior of the cabin and it eliminates the hazards in the cabin of toxic gases and the effects on other electrical equipment caused by radio-frequency interference (RFI) from the laser discharge. However, absorption of the beam as it propagates over the path from the laser to the cabin window, by the oxygen in air at 1 atm, reduces the pulse energy of the beam to 15% of its initial value in 5 m. Therefore, either the loss of laser pulse energy must be offset by increased electrical power to the laser or most of the tubing enclosing the beam from the laser to the cabin window must be partially evacuated or filled with a nonabsorbing gas such as nitrogen. In addition, distortions of the airframe during entry are expected to deflect the beam laterally by 2-3 cm over the path length from the payload bay. Therefore, one or more actively adjusted mirrors will be required in the optical path. However, the distortion

frequencies are believed to be below 1 Hz, allowing simple low-frequency beam-steering devices and sensors to be used.

An alternative location for the laser is in the storage area next to the window, where it would be close to the collection optics. The laser system and its gas supply would be enclosed in a container that is pressure-sealed to reduce the toxic gas hazard and electromagnetically sealed to minimize the RFI. This location would require that electrical power and coolant be brought to the laser from the payload bay and it would reduce the storage capacity of the cabin. This location has the advantage that the optical path of the laser beam to the window-mounted optics is short and insensitive to the effects of cabin-oxygen absorption and airframe distortions during entry.

Once all of the components are in place, the laser gas-filling process, laser start up, and data acquisition can be controlled by a small microprocessor without further attendance during entry.

Laboratory Experiments

Stratosphere Simulator Facility

To verify this concept at conditions that reproduce the optical conditions and signal levels expected in flight, a Stratosphere Simulator Facility was constructed. It was used specifically to demonstrate the capability of a representative instrument system and its associated electronics to achieve the expected signal levels and their linear variation with density, and to demonstrate an ability to obtain signal-to-noise ratios which are near the predicted values and are limited primarily by photon-statistical noise. Except for the indefinite effects of solar background light and aerosol scattering, such a demonstration is sufficient to verify the predicted performance capabilities shown in Fig. 4 and to allow the confident specification of flight instrumentation.

The facility is a 21-meter-long vacuum vessel with an inside diameter of 60 cm. One end-flange has an optical replica of the crew-hatch window mounted in it, including three panes having the identical material, spacings, apertures, and thicknesses as the Shuttle window. However, unlike the configuration shown in Fig. 2, the laser beam was injected into the vessel through a separate small beam-entrance window located at the end of a 260-cm-long tube

with internal apertures. The tube allowed the beam to enter the vessel at the side of the main window, 9 cm from the center-line, and propagate along its length to the center of the opposite end. This method of injection columnated the forward-scattered light from the beam-entrance window and reduced the portion that could reach the interior walls of the vessel and scatter back into the collection optics. In the flight case, no vessel walls would be present to create such a background source and the configuration shown in Fig. 2 could be used.

The vessel is pumped by a 6-inch oil-diffusion pump and can be held at any constant pressure over the range from 1 atm to below 10^{-5} torr, thereby simulating atmosphere densities at all altitudes up to 125 km.

The laser used with this facility is a Questek, model 2260, ArF system with unstable-resonator optics. This laser serves only as a laboratory demonstration device and was not designed with a minimum size and weight. However, its physical configuration and electrical performance are representative of a flight-rated system operating at the highest average power considered because its maximum average power at 100 Hz is slightly greater than the 5 W (50 mJ/pulse) case shown in Fig. 4. Moreover, its power supply is contained within the laser cabinet, the laser is effectively enclosed in RFI shielding, and the gas-fill cycle and average power is controlled by a microprocessor. The laser is 1.4-m long, it occupies a volume of 0.5 m^3, and it weighs 255 kg.

In one series of tests, the ArF laser operating at 50 mJ per pulse and 100 Hz required 2.5 kW of electrical power (3.6 kVA and a power factor of 0.70) from a single-phase 208 V source. It was operated for 45 minutes at those conditions using a single gas-fill with no gas purification or addition. These results demonstrate that the ArF laser can operate unattended over the duration of a Shuttle entry.

At an average laser power of 0.6 W, which was obtained with a pulse energy of 20 mJ at 30 Hz, the ArF laser required 1.1 kW (1.6 kVA) of electrical power. At this condition the laser is 3.6 times less efficient and is operating below its recommended minimum pulse energy. Therefore, a laser that is designed for this lower average laser power may require less than 1.1 kW of electrical power. However, the minimum electrical power that was required by the idling power supply with no laser output or high voltage discharge was

350 W. These results suggest that the minimum electrical power required for any laser in this performance range can be expected to approach 1 kW.

Performance Verification Experiments

In addition to the laser and collection optics already described, the demonstration system included a Hamamatsu R2083Q PMT with a fused-silica envelope and a bi-alkali photocathode, for detection of the Rayleigh light. Its nominal characteristics and those of the band-pass filter are given in Table 2. A reference signal to normalize the Rayleigh signal was obtained with a Hamamatsu R1193U-02 bi-planar photodiode that detected an attenuated fraction of the entire laser beam cross section.

Both signals were integrated using a Stanford Research Systems model SR250 Boxcar Averager. The Rayleigh signal waveform was integrated over a gate period of 80 ns, starting just prior to its initial rise. A much larger signal, owing to the laser beam which was reflected from the far end of the vacuum vessel, arrived after 140 ns and did not affect the Rayleigh-signal integral during the gate period. The reference signal was integrated over a 20-ns period which bracketed the laser pulse and provided an integral which was proportional to the total pulse energy. Both the Rayleigh and reference integrals for each laser pulse were digitized with 12-bit resolution and transferred via a IEEE-488 GPIB interface to an IBM-AT computer where their ratio was computed. At each test condition, data sets for 2000 pulses were stored. Their average ratio and its standard deviation were subsequently computed. The combination of digitizing and normalizing processes limited the resolution of the normalized Rayleigh integral to 0.1% of full scale.

Signal Background and Linearity

The variation of the normalized-Rayleigh-integral (NRI) signal with density was evaluated by varying the vessel pressure. At pressures below 10^{-2} torr, the NRI signal was entirely dominated by background scattering of laser light from the vessel walls. The background came from highly divergent side lobes on one transverse axis of the laser beam which were the consequence of amplified low-angle internal reflections from the electrode rails in the laser. Although the effects of the side lobes were reduced using spatial filtering of the beam, the background scattering caused by them could not be

entirely eliminated. However, when the average background contribution which was measured at vessel pressures below 10^{-4} torr was subtracted from the average total NRI signals obtained at pressures above 10^{-2} torr, the variation was linear with vessel pressure within the resolution of the measurement system. Such corrections would not be necessary in the flight application both because an improved laser cavity design could be implemented which would eliminate the side lobes and because no vessel walls would be present for them to scatter from.

At vessel pressures greater than 30 torr, a reduction of the average NRI signal below that for a linear variation was also observed. This effect occurred in air, but not in nitrogen and is the consequence of absorption of the laser beam by oxygen. However, a vessel pressure of 30 torr corresponds to an equivalent density altitude of 24 km, which is much lower than the minimum altitude at which this technique is applicable. Hence, in the altitude range of interest, absorption of the laser beam by oxygen will have no effect on the linearity of the signal variation with density.

Signal-to-Noise Ratios

The SNR for a single laser pulse is accurately determined by the ratio of the average NRI signal and its standard deviation for 2000 pulses. The experimental results are shown in Fig. 5 for the relevant range of vessel pressures. The equivalent density-altitude corresponding to each vessel pressure is also indicated. The laser was located 5 m from the photodetection electronics and operated at 20 Hz. The energy per pulse at the entrance window to the vessel was 10 mJ. The symbols represent measurements made with various PMT gains. They were adjusted to keep the signal within the range dictated by the maximum anode current at which the PMT is linear and the lowest signal which is accurately resolved by the digital processing. The error bars on the symbols represent the uncertainty owing to the digital resolution of the entire data reduction process at each condition.

The open symbols in Fig. 5 represent measurements made without any additional filters in the optical system. Above 0.1 torr, they show the data to follow a line with a slope of 0.5 on this log-log plot, as it should if the noise is limited mainly by photon-statistics according to Eq. (12). However, below 0.1 torr, the SNR departs from the line as the average NRI approaches

the lower limit caused by the background. Figure 5 also shows an electronic upper limit owing to the minimum noise that can be observed with the digital resolution in use.

Since the SNR data which are not significantly affected by the background signal appear to behave according to Eq. (12), the performance of the system at pressures lower than the minimum allowed by the background can be characterized by placing a neutral density (ND) filter over the face of the PMT. It attenuates the background and reduces the Rayleigh signal to that corresponding to a lower pressure, while having no effect on electrical noise sources such as RFI from the laser. Data taken with the ND filter are represented in Fig. 5 by the closed symbols. The equivalent pressures were determined by using the decrease in SNR of the background signal, measured at pressures below 10^{-4} torr, to calibrate the effective attenuation of the ND filter. The data taken with the filter were then associated with their equivalent pressure without further adjustment. The results merge with the unfiltered data as expected and provide an extension of the results over the full pressure range of interest.

An estimated SNR line is also shown in Fig. 5. It was calculated for the experimental conditions using the nominal parameters of each component in the system in the same manner used for the flight performance predictions. Its agreement with the experimental data is well within the combined uncertainty associated with those parameters. This result, taken in combination with the indication that the SNR data are limited primarily by photon-statistical noise, suggests that the experimental photon flux and the collection efficiency of the photo-detection system are also in agreement with predictions. Hence, these results provide confidence that the performance estimates of the flight instrument shown in Fig. 4, are reasonable expectations.

Summary

An instrument system based on the use of Rayleigh scattering from an ArF laser is shown to be capable of providing direct measurements of atmospheric density during Space Shuttle entry with an uncertainty of less than 1% and with a spatial resolution of 1 km, over an altitude range from 50 to 90 km. Measurements at higher altitudes to 100 km, which extend into low-density-flow

regime of the Shuttle, can also be obtained but with greater uncertainties and lower spatial resolution.

The ultraviolet wavelength of 193 nm from the ArF excimer laser is shown to be the most favorable choice for this application because of the larger Rayleigh signal and the lower solar background that occur at shorter wavelengths. To test an alternative laser choice, a frequency-quadrupled Nd:YAG laser operating at 266 nm is also considered and shown not to be adequate for this application because of the loss of performance owing to the longer wavelength.

The primary parameter that characterizes the laser performance for this application is its average power. An ArF laser that is operating at an average power of 0.6 W is shown to be adequate for providing the required measurements. However, that average power is much less than the maximum capabilities of most commercial excimer lasers and the performance of the system can be enhanced considerably by using a readily available laser with an average power of 5 W.

The vehicle utilities required to support an ArF laser that is operating at 0.6 to 5 W have been implied from tests using a commercial laser. The results show that the required electrical power is expected to be in the range between 1 - 2.5 kW. In addition, the laser with its power supply and gas supply could weigh up to 300 kg and will require liquid coolant at flow rates up to 4 l/min.

Experimental measurements were performed in a simulator facility at conditions that duplicated the flight environment. They confirmed the ability of an instrument system which was assembled from commercially-available equipment to meet the necessary performance requirements. The experimental results demonstrate the achievement of signal-to-noise ratios that are limited primarily by photon statistics and with values near those predicted for the experimental conditions. From these results, the design requirements of a flight system can be specified with confidence.

Acknowledgement

The author is grateful to Francis X. Hurley, former NASA Deputy Chief Scientist, whose advocacy made this project possible, to Frank P. Scholz,

Rockwell International, for many helpful discussions, and to Bruce Banfield, NASA Ames, for his assistance in the mechanical design of the Stratosphere Simulator Facility.

References

[1]U.S. Standard Atmosphere, 1976, NOAA, NASA, USAF, NOAA-S/T 76-1562, 1976.

[2]Hines, C.O., "Internal Atmospheric Gravity Waves at Ionospheric Heights," Can. J. Phys., Vol.38, 1960, pp. 1441-1481.

[3]Lindzen, R.S., "Turbulence and Stress Owing to Gravity Wave and Tidal Breakdown," J. Geophysical Res., Vol.86, Oct. 1981, pp. 9707-9714.

[4]Rastogi, P.K. and Bowhill, S.A., "Scattering of Radio Waves from the Mesosphere--2. Evidence for Intermittent Mesosphere Turbulence," J. Atm. Terr. Phy., Vol.38, 1976, pp.449-462.

[5]Findley, J.T., Kelly, G.M., and Troutman, P.A., "Final Report - Shuttle Derived Atmosphere Density Model (Parts 1 and 2)," NASA CR 171824, Dec. 1984.

[6]Blanchard, R.C., and Rutherford, J.F., "Shuttle Orbiter High Resolution Accelerometer Package Experiment: Preliminary Flight Results," J. Spacecraft and Rockets, Vol.22, No.4, July 1985, pp474-480.

[7]Talay, T.A., White, N.H., and Naftel, J.C., "Impact of Atmospheric Uncertainties and Viscous Interaction Effects on the Performance of Aero-Assisted Orbital Transfer Vehicles," AIAA Paper 84-0408, Jan. 1984.

[8]Price, J.M., and Blanchard, R.C., "Determination of Atmospheric Properties for STS-1 Aerothermodynamic Investigations," AIAA Paper 81-2430, Nov. 1981.

[9]Compton, H., Findley, J., Kelly, G., and Heck, M., "Shuttle (STS-1) Entry Trajectory Reconstruction," AIAA Paper 81-2459, Nov. 1981.

[10]Siemers III, P.M., Wolf, H., and Flanagan, P.F., "Shuttle Entry Air Data System Concepts Applied to Space Shuttle Orbiter Flight Pressure Data to Determine Air Data - STS 1-4," AIAA Paper 83-0118, Jan. 1983.

[11]Pruett, D.C., Wolf, H., Heck, M.L., and Siemers III, P.M., "Innovative Air Data System for thr Space Shuttle Orbiter," J. Spacecraft and Rockets, Vol.20, No.1, Jan. 1983, pp. 61-69.

[12]Blanchard, R.C., Duckett, R.J., and Hinson, E.W., "The Shuttle Upper Atmosphere Mass Spectrometer Experiment," J. Spacecraft and Rockets, Vol.21, No.2, Mar. 1984, pp. 202-208.

[13]Siemers III, P.M., NASA Langley Research Center, private communication.

[14]McKenzie, R.L., "A Method of Atmospheric Density Measurement During Shuttle Entry Using UV Laser Rayleigh Scattering," AIAA Paper 87-1530, June, 1987.

[15]Samson, J.A.R., "On the Measurement of Rayleigh Scattering," J. Quant. Spectrosc. Radiat. Transfer, Vol.9, 1969, pp. 875-879.

[16]Shardanand and Rao, A.D.P., "Absolute Rayleigh Scattering Cross Sections of Gases and Freons of Stratospheric Interest in the Visible and Ultraviolet Regions," NASA Tech. Note D-8442, Mar. 1977.

[17]Penndorf, R., "Tables of the Refractive Index for Standard Air and the Rayleigh Scattering Coefficient for the Spectral Region between 0.2 and 20.0 f and Their Application to Atmospheric Optics," J. Optical Soc. of Amer., Vol.47, No.2, Feb. 1957, pp. 176-182.

[18]Edlen, B., "The Dispersion of Standard Air," J. Optical Soc. Amer., Vol.43, No.5, May 1953, pp. 339-344.

[19]Taylor, D.J., Los Alamos National Laboratory, private communication.

[20]Lewis, B.R., Berzins, L., Carver, J.H., and Gibson, S.T., "Rotational Variation of Predissociation Linewidth in the Schumann-Runge Bands of 1602," J. Quant. Spectros. Radiat. Transfer, Vol. 36, No. 3, 1986, pp. 187-207.

[21] Lewis, B.R., Berzins, L., and Carver, J.H., "Oscillator Strengths for the Schumann-Runge Bands of 1602," J. Quant. Spectros. Radiat. Transfer, Vol. 36, No. 3, 1986, pp. 209-232.

[22]Prabhu, D.K. and Tannehill, J.C., "Numerical Solution of Space Shuttle Orbiter Flowfield Including Real-Gas Effects," J. Spacecraft and Rockets, Vol.23, No.3, May 1986, pp.264-272.

[23]Chaussee, D.J., NASA Ames Research Center, private communication.

[24]Goodrich, W.D., NASA Johnson Space Center, private communication.

[25]"Laser Focus Buyers' Guide, 1987," Pennwell Pub. Co. Litteton, MA.

[26]Thekaekara, M.P., "Extraterrestrial Solar Spectrum, 3000-6100 A at 1-A Intervals," Applied Optics, Vol.13, No.3, Mar. 1974, pp. 518-522.

[27]Plass, G.N. and Kattawar, G.W., "Calculations of Reflected and Transmitted Radiance for Earth's Atmosphere," Applied Optics, Vol.7, No.6, June 1968, pp. 1129-1135.

[28]van de Hulst, H.C., "Light Scattering by Small Particles," J. Wiley and Sons, New York, 1957.

[29]McClatchey, R.A., Fenn, R.W., Selby, J.E.A., Volz, F.E., and Garing, J.S., "Optical Properties of the Atmosphere," in Handbook of Optics, Section 14, McGraw-Hill, 1978.

[30]Volz, F.E., "Infrared Refractive Index of Atmospheric Aerosol Substances," Applied Optics, Vol.11, No.4, Apr. 1972, pp. 755.

[31]Deirmendjian, D., "Scattering and Polarization Properties of Water Clouds and Hazes in the Visible and Infrared," Applied Optics, Vol.3, No.2, Feb. 1964, pp. 187-196.

[32]Hunten, D.M., Turco, R.P., and Toon, O.B., "Smoke and Dust Particles of Meteoric Origin in the Mesosphere and Stratosphere," J. Atmos. Sci., Vol.37, June 1980, pp. 1342-1357.

[33]Whitten, R.C., (Editor), "The Stratospheric Aerosol Layer," Topics in Current Physics, Vol. 28, Springer-Verlag, New York, 1982.

[34]Kingston, R.H., "Detection of Optical and Infrared Radiation," Springer-Verlag, New York, 1978.

Figure Titles

Fig. 1 The variability of density from the U.S. Standard Atmosphere, 1976, The extremes amplitudes shown are those which occur with 1% probability. (From Ref. 1).

Fig. 2 The configuration of the laser transmitter optics and the scattered-light collection optics which are mounted on the interior of the crew hatch window on the Shuttle middeck.

Fig. 3 The wavelength dependence of factors affecting the measurement performance. The symbols mark the wavelengths at 193 nm and 266 nm of the two lasers evaluated.

Fig. 4 Variations of the signal-to-noise ratio with altitude for a spatial resolution of 1 km.

Fig. 5 Experimental and estimated signal-to-noise ratios in the Stratosphere Simulator Facility using an ArF laser operating at a wavelength of 193 nm and a pulse energy of 10 mJ. The SNR data correspond to single-pulse values derived from 2000-pulse averages.

Table 1 Methods of Atmospheric Density Determination Along the Space Shuttle Flightpath

Instrument	Type/reference	Primary Objective	Altitude range	Density uncertainty	Comments
Radiosonde/ LAIRS	Rocket-launched probes, spheres[8]	Upper atmosphere temperature and density	30 - 90 km	3-5%	Data not on flight path nor taken at time of flight
IMU/BET	3-axis accelerometers[9]	Vehicle dynamics	0 - 90 km	3-5%	Depends on known aerodynamic coeffs.
SEADS	Pressure orifices in Shuttle nose[10,11]	Free-stream dynamic pressure, angle of attack	0 - 95 km	3-4%	Currently most accurate air-data instrumentation
SUMS	Mass spectrometer[12]	Free-stream density, gas composition	90 - 130 km	10-20%	Only instrument with capability in rarefied flight regime
HiRAP	Very low-level accelerometers[6]	Vehicle dynamics in low-density regime	90 - 160 km	5-20%	Used in conjunction with SUMS for high altitude density determinations
This method	UV Rayleigh scattering	Free-stream density	50 - 90 km	<1%	Independent of other flight or atmosphere data

Acronym definitions:

BET: Best estimated trajectory (data analysis procedure)

HiRAP: High resolution accelerometer package

IMU: Inertial measurements unit

LAIRS: Langley atmosphere information retrieval system (computer code)

SEADS: Langley entry air data system

SUMS: Shuttle upper atmosphere mass spectrometer

Table 2 Detector Characteristics

Photomultiplier Tube -

Photocathode material: CsTe on UV fused silica

Quantum Efficiency: 15% from λ = 193 to 266 nm

Rise time: 0.7 ns

Minimum gain: 1×10^3 at 800 Volts

Maximum gain: 2×10^6 at 3500 Volts

Maximum peak anode current: 20 mA

Maximum average anode current: 0.2 mA

Filter -

Peak transmission: 16%

Bandpass: 22nm (FWHM)

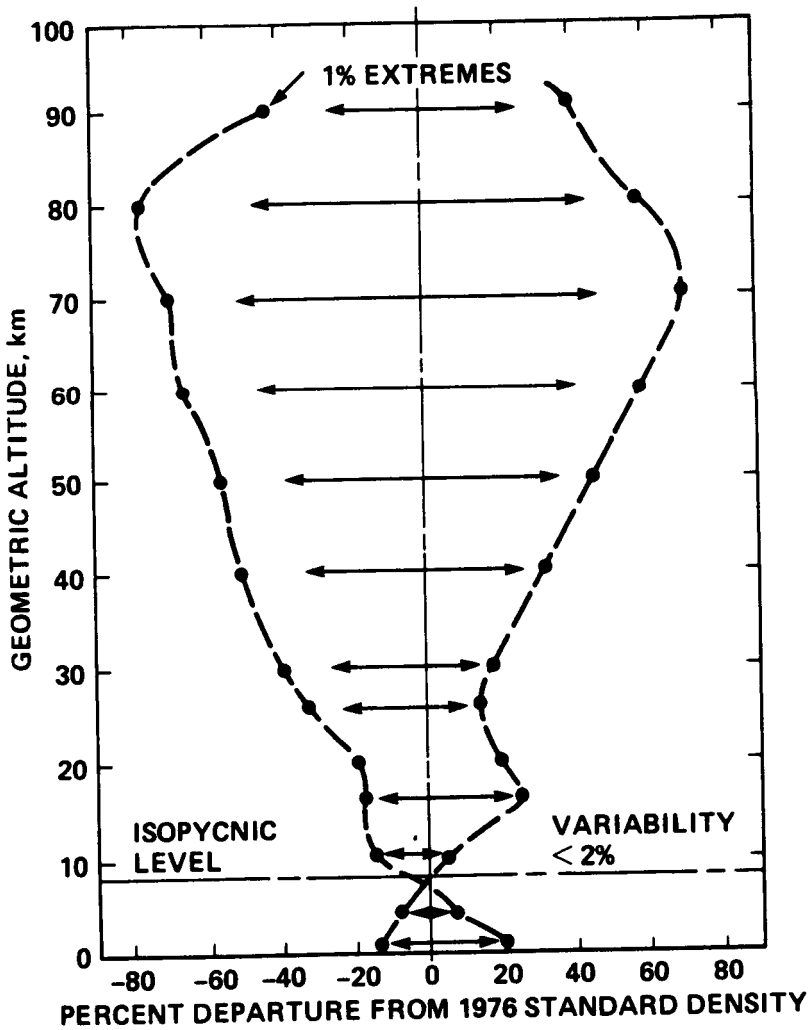
100
90
80
70
60
50
40
30
20
10
0
GEOMETRIC ALTITUDE, km
1% EXTREMES
ISOPYCNIC
LEVEL
VARIABILITY
< 2%
-80
-60
-40
-20
0
20
40
60
80
PERCENT DEPARTURE FROM 1976 STANDARD DENSITY

fig.1

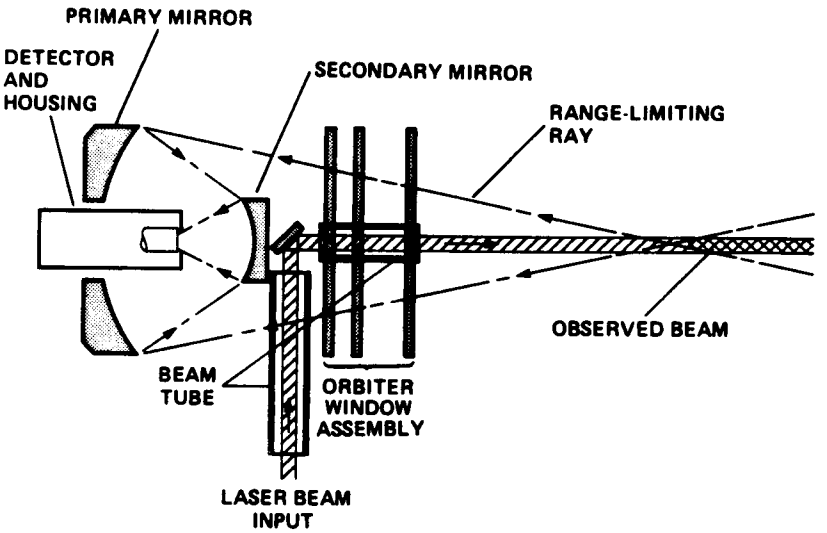
PRIMARY MIRROR
DETECTOR AND HOUSING
SECONDARY MIRROR
RANGE-LIMITING RAY
OBSERVED BEAM
BEAM TUBE
ORBITER WINDOW ASSEMBLY
LASER BEAM INPUT

fig.2

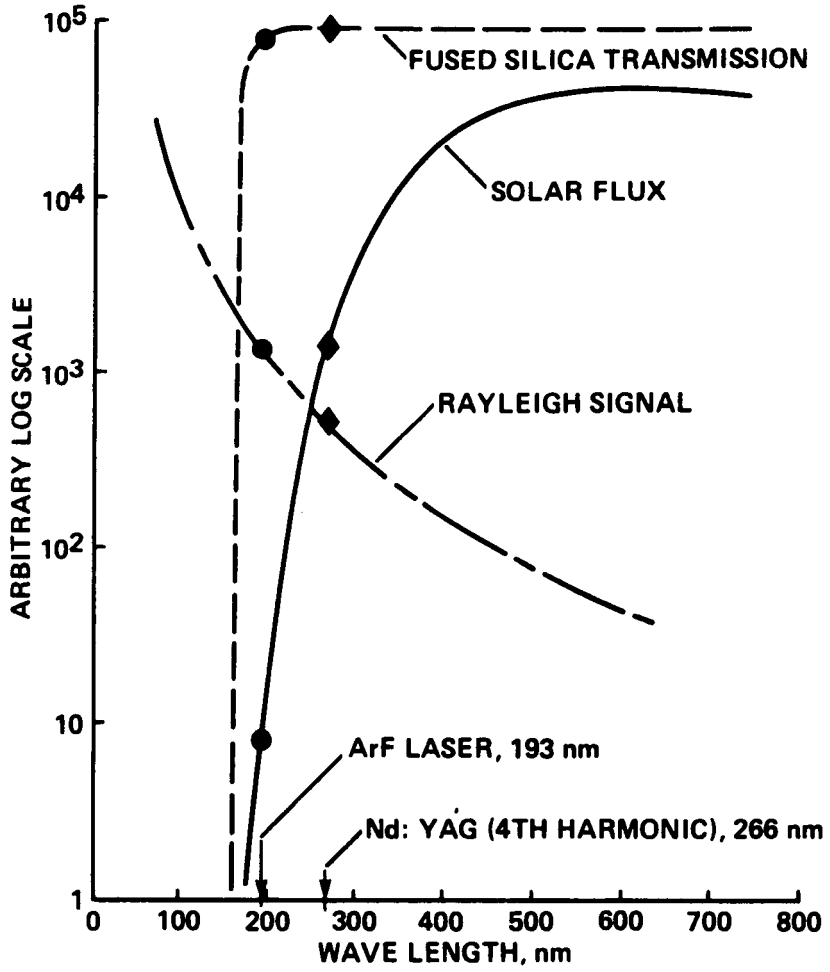
FUSED SILICA TRANSMISSION
SOLAR FLUX
RAYLEIGH SIGNAL
ArF LASER, 193 nm
Nd: YAG (4TH HARMONIC), 266 nm
ARBITRARY LOG SCALE
10^5
10^4
10^3
10^2
10
1
0
100
200
300
400
500
600
700
800
WAVE LENGTH, nm

fig.3

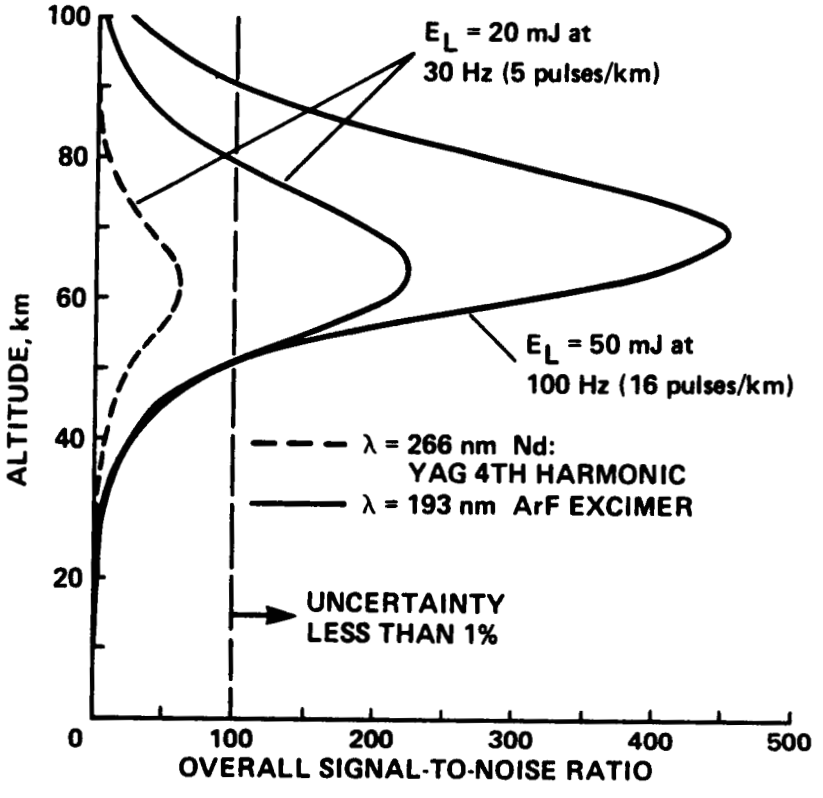
100
80
60
40
20
0
ALTITUDE, km
100
200
300
400
500
OVERALL SIGNAL-TO-NOISE RATIO
E_L = 20 mJ at
30 Hz (5 pulses/km)
E_L = 50 mJ at
100 Hz (16 pulses/km)
λ = 266 nm Nd:
YAG 4TH HARMONIC
λ = 193 nm ArF EXCIMER
UNCERTAINTY
LESS THAN 1%

fig. 4

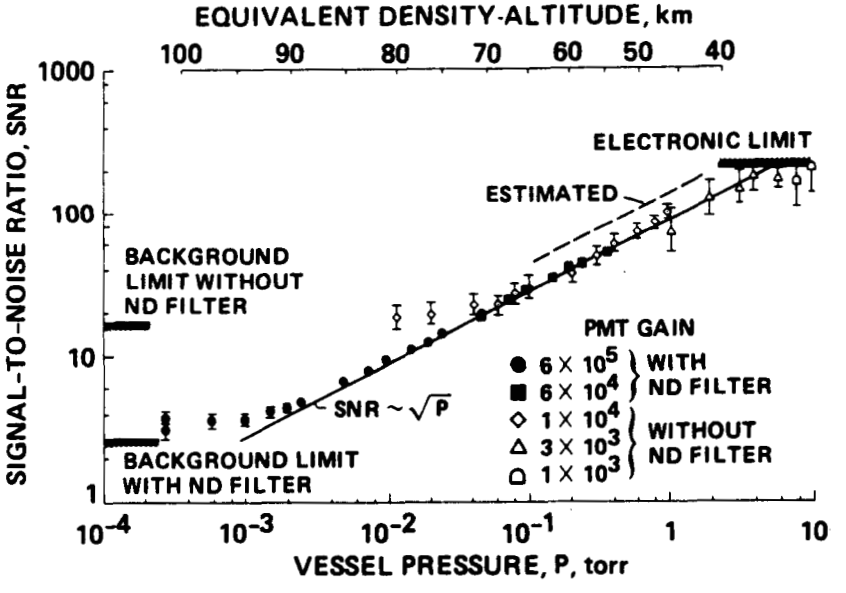
EQUIVALENT DENSITY-ALTITUDE, km
100
90
80
70
60
50
40
1000
100
10
1
SIGNAL-TO-NOISE RATIO, SNR
ELECTRONIC LIMIT
ESTIMATED
BACKGROUND
LIMIT WITHOUT
ND FILTER
SNR ~ √P
BACKGROUND LIMIT
WITH ND FILTER
PMT GAIN
6 X 10^5
6 X 10^4
WITH
ND FILTER
1 X 10^4
3 X 10^3
1 X 10^3
WITHOUT
ND FILTER
10^-4
10^-3
10^-2
10^-1
1
10
VESSEL PRESSURE, P, torr

fig. 5

NASA National Aeronautics and Space Administration

Report Documentation Page

1. Report No.	2. Government Accession No.	3. Recipient's Catalog No.
NASA TM 100056		

4. Title and Subtitle

A Method of Atmospheric Density Measurements During Space Shuttle Entry Using Ultraviolet-Laser Rayleigh Scattering

5. Report Date

March 1988

6. Performing Organization Code

7. Author(s)

Robert L. McKenzie

8. Performing Organization Report No.

A-88058

10. Work Unit No.

506-40-4

9. Performing Organization Name and Address

NASA Ames Research Center
Moffett Field, CA 94035

11. Contract or Grant No.

13. Type of Report and Period Covered

Technical Memorandum

12. Sponsoring Agency Name and Address

National Aeronautics and Space Administration
Washington, DC 20546-0001

14. Sponsoring Agency Code

15. Supplementary Notes

Point of Contact: Robert McKenzie, Ames Research Center, MS 229-1, Moffett Field, CA, (415) 694-6158 or FTS 464-6158

16. Abstract

An analytical study and its experimental verification are described which show the performance capabilities and the hardware requirements of a method for measuring atmospheric density along the Space Shuttle flightpath during entry. Using onboard instrumentation, the technique relies on Rayleigh scattering of light from a pulsed ArF excimer laser operating at a wavelength of 193 nm. The method is shown to be capable of providing density measurements with an uncertainty of less than 1% and with a spatial resolution along the flightpath of 1 km, over an altitude range from 50 to 90 km. Experimental verification of the signal linearity and the expected signal-to-noise ratios is demonstrated in a simulation facility at conditions that duplicate the signal levels of the flight environment.

17. Key Words (Suggested by Author(s))	18. Distribution Statement
Density measurements Laser Rayleigh scattering Space Shuttle instrumentation	Unclassified - Unlimited Subject category: 35

19. Security Classif. (of this report)	20. Security Classif. (of this page)	21. No. of pages	22. Price
Unclassified	Unclassified	35	A03

For sale by the National Technical Information Service, Springfield, Virginia 22161